

Phase-Preserving ScanSAR Image Generation

R. Lanari⁽¹⁻²⁾, S. Hensley⁽²⁾, P. A. Rosen⁽²⁾

⁽¹⁾IRECE-CNR, via Diocleziano 328, 80124 Napoli, Italy
+ 39-(0)81-5707999 - fax. +39-(0)81-5705734
c-mail: lanari@irece1.irece.na.cnr.it

⁽²⁾ Jet propulsion Laboratory, 4800 Oak Grove Drive,
Pasadena, CA 91109, USA

Abstract

The scan mode synthetic aperture radar (ScanSAR) image impulse response is derived in the time-domain and particular attention is given to the analysis of the phase, which is important for several applications, and especially in interferometric ScanSAR systems. The signal spectral characteristics are also discussed.

A new phase-preserving Scan SAR processing algorithm that extends the SPECAN procedure is presented; the proposed algorithm avoids the interpolation step needed to achieve a constant azimuth pixel spacing by replacing the standard Fourier transform used in the SPECAN procedure with an appropriate chirp z-transform.

The relationship between the modified SPECAN algorithm and the standard range-Doppler approach is also discussed. Experiments on simulated data are carried out to validate the theory.

Submitted to the special issue on Spectral Analysis Applications in Radar (IEE Proc. on Radar, Sonar and Navigation)

I. Introduction

Synthetic aperture radar (SAR) is a coherent imaging sensor that allows the generation of high resolution microwave images. SAR systems currently operate on both airborne and spaceborne platforms and synthesize a long antenna, in the platform flight direction (often referred to as along track or azimuth direction), by transmitting pulsed signals and coherently adding the backscattered echoes [1]. The antenna synthesis operation is generally carried out digitally and high azimuth resolutions (of the order of meters/tens of meters) are achieved. In the across track (range) direction high resolutions are obtained by transmitting either very short pulses or properly coded signals; in the latter case a processing operation, generally referred to as *range compression*, is required based on the convolution of the received echo with the conjugate, time-inverted, replica of the transmitted signal.

The most common operating mode for a SAR sensor is the strip mode, where the radar antenna pointing direction is fixed with respect to the platform flight track and the illumination footprint covers a strip on the ground as the platform moves. The finest azimuth resolution is independent of the sensor-target range and is equal to half of the physical antenna length in the azimuth direction [2].

In principle, for the strip mode SAR configuration, the extent of the mapping swath in the along track direction is arbitrarily long while the range swath is fundamentally constrained by the length of time between successive pulses [1-2], called the pulse repetition interval (PRI). If images with large range swaths are required it is possible to overcome the strip mode limitation by using the scan SAR (ScanSAR) mode [3-4]. In this case the sensor antenna beam is periodically stepped in range to neighbouring swaths referred to as sub-swaths. As a consequence the overall range swath dimension is increased however, for each target, only portions of the full synthetic antenna length are collected. In the Scan SAR case the range swath width increases at the expense of the azimuth resolution since full antenna synthesis is no longer possible.

In this work we investigate the ScanSAR image impulse response characteristics. Particular attention is given to the analysis of the phase

which is important for several applications, including, interferometry, polarimetry, etc.. An immediate application of ScanSAR interferometry is the Shuttle Radar Topography Mission (SRTM), scheduled to fly in 1999. In this case, in order to map the entire landmass between $\pm 60^\circ$ of latitude within a ten days mission, it is necessary to operate the shuttle radar in a ScanSAR mode [5].

We also present a new phase-preserving algorithm for Scan SAR data processing that extends the SPECAN procedure [6] and represents a candidate for SRTM. The proposed approach avoids the range dependent scaling of the azimuth pixel dimension of the ScanSAR images obtained when applying the basic SPECAN procedure. This result, achieved in the SPECAN approach via a post-processing interpolation step, is obtained in our case by simply replacing the standard Fourier transform (FT) used in the SPECAN algorithm with one whose kernel includes a range-dependent correction factor. This transform is implemented via a chirp z-transform [7] that can be efficiently carried out via fast Fourier transform (FFT) codes. ScanSAR images generated using the modified SPECAN algorithm have a constant azimuth pixel spacing whose dimension can be selected according to the application requirements.

The paper is organized as follows: section II is dedicated to the time-domain ScanSAR image generation analysis that will be used as a reference in the succeeding sections. The frequency domain analysis is presented in section III to clarify the spectral properties of the signal. Section IV is dedicated to the chirp z-transform based processing approach. Experimental results validate the overall analysis.

II. Time-domain analysis

Considering the cylindrical coordinate system geometry (x, r, ϑ) shown in fig. 1. The x axis is coincident with the platform flight path previously defined to as azimuth direction; r and ϑ are usually referred to as the closest approach distance and look angle, respectively. We assume the platform trajectory to be a straight line (see fig. 1), appropriate for airborne but not for spaceborne sensors. However it can be shown that spaceborne data can be processed in the same manner as

airborne data if the closest approach distance and the azimuth velocity are properly considered [8].

Assume that the sensor platform moves at a constant velocity $\underline{v} = v \hat{x}$ and the radar transmits pulsed signals; although the radar is continuously pulsing, the antenna beam is periodically stepped in the range direction to illuminate neighbouring sub-swaths (see fig. 2 for a two sub-swaths example). The interval when the antenna beam illuminates a particular sub-swath is referred to as *burst* and its duration is denoted as T_B ; the interval separating the start of successive bursts illuminating the same sub-swath is the burst period, T_p . Note that in order to guarantee continuous coverage along the flight direction the burst period needs to be smaller than the synthetic aperture time extent $T_S = X_S / v$ where X_S is the synthetic aperture length, assumed equal to the (azimuth) 3-dB antenna footprint. The ratio:

$$N_L = \frac{T_S}{T_p} \quad (1)$$

is usually referred to as the number of looks and represents the number of bursts to which the backscattered signal of a single target contributes.

Assume that the radar transmits *chirped* pulses of duration τ , at times $t_n - \tau/2$, given by:

$$f_1(t - t_n) = \exp \left[j \omega (t - t_n) - j \frac{\alpha}{2} (t - t_n)^2 \right] \text{rect} \left[\frac{t - t_n}{\tau} \right] \quad (2)$$

wherein ω is the angular carrier frequency and α is the chirp rate satisfying the equation $\alpha \tau = 2\pi \Delta f$ wherein Δf is the chirp bandwidth. Selection of the chirp waveform is not fundamental for the following analysis but it has been done since it is used by almost all operating SAR sensors.

If we consider the elementary scatterer $S \equiv (x, r, \vartheta)$ the received ~~scattered~~ (excluding an ~~amplitude~~ amplitude factor) is:

$$\begin{aligned}
f(t^- t_n, x' - x, r, x) &= f\left(t - t_n - \frac{2R}{c}\right) w^2 \left[\frac{x' - x}{X_S} \right] \sum_{l=-\infty}^{+\infty} \text{rect} \left[\frac{x' - lX_P}{X_B} \right] \\
&= \exp \left[j \omega \left(t - t_n - \frac{2R}{c} \right) - j \frac{\alpha}{2} \left(t - t_n - \frac{2R}{c} \right)^2 \right] \\
&\quad \cdot \text{rect} \left[\frac{t - t_n - \frac{2R}{c}}{\tau} \right] w^2 \left[\frac{x' - x}{X_S} \right] \sum_{l=-\infty}^{+\infty} \text{rect} \left[\frac{x' - lX_P}{X_B} \right]
\end{aligned} \tag{3}$$

where.

$$R = \sqrt{(x' - \bar{x})^2 + r^2} \approx r + \frac{(x' - \bar{x})^2}{2r}, \tag{4}$$

is the target-platform distance,

$$x' = vt_n, \quad X_B = vT_B, \quad X_P = vT_P, \tag{5}$$

c is the speed of light, $w[\cdot]$ represents the antenna pattern and is squared because the same antenna is used both for transmitting and receiving; the term $\text{rect}[x' - lX_P / X_B]$ in the summation operator of eq. (3) accounts for the burst windowing. Note that since the burst is generally very short the Taylor expansion in eq. (4) is valid; moreover we simplify the analysis by assuming no squint (or equivalently no Earth rotation induced effects) however the extension of eq.(3) to a squinted geometry only requires introducing the new antenna pattern expression $w^2 \left[(x' - x + r \tan \phi_0) / X_S \right]$ where ϕ_0 is the squint angle⁽¹⁾. Note also that the relationship among X_B, X_P and X_S is shown in fig. 3.

Due to the *burst* nature of the ScanSAR signal the data processing is generally carried out by separately focusing the single bursts and then incoherently combining them⁽²⁾; this is the case if intensity images

(1) We **assumed** in this case a flat Earth profile.

(2) An **alternative solution** proposed in [9] and based on the **strip mode processing** of long **burst trains** with zeroes inserted between **bursts** is **not** considered here.

are desired and explains why the factor N_l in eq. (1) is referred to as the number of looks. On the other hand, in the interferometric Scan SAR case, the processing procedure is generally performed burst by burst but it must be carried out up to the interferogram generation; at this stage the interferograms of the different looks can be combined (complex multilook).

Therefore we focus our attention on a single burst. In order to simplify the notation we select the burst obtained by assuming $l = 0$ in the summation operation in eq. (3). Defining in eq. (3) the *range* variable $r' = (f - t_n)c/2$, after range compression we have:

$$\begin{aligned}
 h(r' - r, x' - x, r, x) &\approx \exp\left(-j\frac{4\pi}{\lambda}r\right) \exp\left[-j2\pi\frac{(x' - x)^2}{\lambda r}\right] w^2\left[\frac{x' - x}{X_S}\right] \cdot \\
 &\cdot \text{rect}\left[\frac{x'}{X_B}\right] \text{sinc}\left[\frac{\pi}{\Delta r}\left(r' - r - \frac{(x' - x)^2}{2r}\right)\right] \\
 &\approx \exp\left(-j\frac{4\pi}{\lambda}r\right) \exp\left[-j2\pi\frac{(x' - x)^2}{\lambda r}\right] w^2\left[\frac{x' - x}{X_S}\right] \cdot \\
 &\cdot \text{rect}\left[\frac{x'}{X_B}\right] \text{sinc}\left[\frac{\pi}{\Delta r}(r' - r)\right],
 \end{aligned} \tag{6}$$

where $\Delta r = c/2Af$ is the range resolution. The fast varying factor $\exp[j\omega(t - t_n)]$ does not appear in eq. (6) because it is removed via a heterodyne operation in the receiver. Moreover, we neglect the effect of the range migration term $(x' - x)^2/\lambda r$, in the argument of the sine function in eq. (6), since, as already stated, the burst length is generally very short and this term is a small fraction of the range resolution cell. Note that if the range migration is not negligible, the following analysis maintains its validity but the data processing procedure requires an additional step whose characteristics depend on the chosen range migration compensation approach. It can be based on a chirp scaling [10], a standard 2D-frequency [11-12] or a range-Doppler algorithm [13].

If we assume, as usual, a high range compression gain, eq. (6) becomes:

$$\begin{aligned}
 h(r' - r, x' - x, r, x) &\approx \exp\left(-j\frac{4\pi}{\lambda}r'\right) \exp\left[-j2\pi\frac{(x' - x)^2}{\lambda r'}\right] w^2\left[\frac{x' - x}{X_S}\right] \\
 &\quad \cdot \text{rect}\left[\frac{x'}{X_B}\right] \text{sinc}\left[\frac{\pi}{\Delta r}(r' - r)\right] \\
 &= a(x' - x, r', x) \exp\left(-j\frac{4\pi}{\lambda}r'\right) \text{sinc}\left[\frac{\pi}{\Delta r}(r' - r)\right],
 \end{aligned} \tag{7}$$

wherein

$$a(x' - x, r', x) = \exp\left[-j2\pi\frac{(x' - x)^2}{\lambda r'}\right] w^2\left[\frac{x' - x}{X_S}\right] \text{rect}\left[\frac{x'}{X_B}\right]. \tag{8}$$

The presence of the burst factor $\text{rect}[x'/X_B]$ causes the backscattered signal to be *azimuthally dependent*, through the explicit x-dependence of the signals $h(\cdot)$ and $a(\cdot)$ in eqs. (7) and (8), respectively. In other words the backscattered signal characteristics do not depend only on where the target is located in range, as in the case of strip mode [10-13], but also on its azimuth location.

We now focus on ScanSAR image generation. According to eq. (7) it is possible to consider the following focusing strategy: we convolve, in the azimuth direction, the range compressed signal with the matched filter of the azimuth component of the strip mode reference function:

$$g(x', r') = \exp\left(j2\pi\frac{x'^2}{\lambda r'}\right) \text{rect}\left[\frac{x'}{X_S}\right], \tag{9}$$

which is *independent* of azimuth since its extent is represented by the overall synthetic antenna length X_S . The convolution is effectively carried out with the function $a(\cdot)$ in eq. (7), therefore we neglect in the following the range component of eq. (7).

Note that the proposed analysis is aimed at the evaluation of the Scan SAR image impulse response characteristics, so at this point computational processing efficiency is not considered. A simple and efficient solution for phase-preserving Scan SAR data processing is presented in section IV.

Mathematically, the azimuth convolution operation can be expressed as follows:

$$\begin{aligned} \tilde{a}(x' - x, r', x) &= a(x' - x, r', x) \otimes_{x'} g(x' - r') \\ &= \left\{ \exp \left[-j2\pi \frac{(x' - x)^2}{\lambda r'} \right] w^2 \left[\frac{x' - x}{X_S} \right] \text{rect} \left[\frac{x'}{X_B} \right] \right\} \otimes_{x'} \\ &\quad \left\{ \exp \left(j2\pi \frac{x'^2}{\lambda r'} \right) \text{rect} \left[\frac{x'}{X_S} \right] \right\} \quad \text{with } \frac{X_B - X_S}{2} \leq x' \leq \frac{X_S - X_B}{2} \end{aligned} \quad (10)$$

wherein symbol $\otimes_{x'}$ represents the azimuth convolution operation and we consider as valid output samples those within the interval $(X_B - X_S)/2 \leq x' \leq (-X_B + X_S)/2$. The limits in the convolution integral are chosen such that if $x = x'$ then signal contributions are obtained for the entire burst duration (see fig. 3). These limits will be assumed throughout unless otherwise specified. Therefore, since the support of the signal is contained within $\text{rect}[x'/X_S]$, we may rewrite eq. (10) as:

$$\begin{aligned} \tilde{a}(x' - x, r', x) &= \left\{ \exp \left[-j2\pi \frac{(x' - x)^2}{\lambda r'} \right] w^2 \left[\frac{x' - x}{X_S} \right] \text{rect} \left[\frac{x'}{X_B} \right] \right\} \otimes_{x'} \\ &\quad \left\{ \exp \left(j2\pi \frac{x'^2}{\lambda r'} \right) \right\}. \end{aligned} \quad (11)$$

Using the fact that the burst length is short with respect to the antenna footprint we may approximate eq. (11) as:

$$\tilde{a}(x' - x, r', x) \approx \left\{ \exp \left[-j2\pi \frac{(x' - x)^2}{\lambda r'} \right] \text{rect} \left[\frac{x'}{X_B} \right] \right\} \otimes_{x'} \left\{ \exp \left(j2\pi \frac{x'^2}{\lambda r'} \right) \right\} \\ \text{“ } w^2 \left[\frac{x'}{X_S} \right] \text{”} \quad (12)$$

Explicitly evaluating the convolution integral in eq. (12) yields

$$\tilde{a}(x' - x, r', x) \approx \left\{ \int ds \text{rect} \left[\frac{s}{X_B} \right] \exp \left[-j2\pi \frac{(s - x)^2}{\lambda r'} \right] \exp \left[j2\pi \frac{(x' - s)^2}{\lambda r'} \right] \right\} \\ \text{“ } w^2 \left[\frac{x'}{X_S} \right] \text{”} \\ = \left\{ \int ds \text{rect} \left[\frac{s}{X_B} \right] \exp \left[j2\pi \frac{2(x' - x)s - s^2 - x^2}{\lambda r'} \right] \right\} \\ \text{“ } w^2 \left[\frac{x'}{X_S} \right] \exp \left[j2\pi \frac{x'^2 - x^2}{\lambda r'} \right] \text{”} \\ = w^2 \left[\frac{x'}{X_S} \right] \exp \left[j2\pi \frac{x'^2 - x^2}{\lambda r'} \right] \text{sinc} \left[2\pi \frac{X_B}{\lambda r'} (x' - x) \right] \\ = w^2 \left[\frac{x'}{X_S} \right] \exp \left[j2\pi \frac{(x' + x)(x' - x)}{\lambda r'} \right] \text{sinc} \left[\frac{2\pi X_B}{L X_S} (x' - x) \right], \quad (13)$$

where an unessential amplitude factor has been neglected and we assumed, as usual, $X_S \approx \lambda r' / L$, where L is the azimuth physical antenna dimension. We note in eq. (13) the azimuth amplitude modulation effect caused by the antenna pattern term $w^2[\cdot]$ usually referred to as scalloping. Compensation of this effect requires the knowledge of the antenna pointing characteristics however an azimuth varying signal to noise ratio is introduced in the image obtained from the burst. If we compensate for the antenna pattern term in eq. (13)

and consider the range component of eq. (7) we finally get the overall ScanSAR image impulse response:

$$I_{SCAN}(r' - r, x' - x, r', x) \approx \exp\left(-j\frac{4\pi}{\lambda}r'\right) \text{sinc}\left[\frac{\pi}{\Delta r}(r' - r)\right] \exp\left[j2\pi\frac{(x' + x)(x' - x)}{\lambda r'}\right] \text{sinc}\left[\frac{2\pi X_S}{L} \frac{X_B}{X_S} (x' - x)\right] \quad (14)$$

Consider the corresponding image impulse response for one sub-swath of a strip mode sensor operating with the same system characteristics. In this case, we get [10-13]:

$$I_{STRIP}(r' - r, x' - x, r') \approx \exp\left(-j\frac{4\pi}{\lambda}r'\right) \text{sinc}\left[\frac{\pi}{\Delta r}(r' - r)\right] \text{sinc}\left[\frac{2\pi}{L}(x' - x)\right]. \quad (15)$$

By comparing eqs. (14) and (15) some observations are immediate. Let us consider first the relationship between the 3-dB azimuth resolutions achieved in the two modes, say Δx_{SCAN} and Δx_{STRIP} :

$$\Delta x_{SCAN} \approx \frac{L}{2} \frac{X_S}{X_B} \approx \Delta x_{STRIP} \frac{X_S}{X_B} > \Delta x_{STRIP} \quad (16)$$

where $\Delta x_{STRIP} \approx L/2$. As expected the burst mode operation leads to an azimuth resolution degradation; in particular it depends on the ratio between the ideal synthetic strip aperture length X_S and the burst length X_B . Since $X_S \approx \lambda r' / L$ depends on r' , the finest achievable azimuth resolution for the scan mode increases from near to far range. Note also that for targets that do not contribute to the backscattered signal for the overall burst length, there is an additional azimuth resolution degradation. This result is easily obtained by redefining X_B in eq. (16) as the effective burst duration within which the

backscattered signal is received. For Scan SAR data with less than two looks these points are needed to ensure the image continuity.

We concentrate now on the phase of eq. (14). By comparing it with that of eq. (15) we note the presence of the additional parabolic factor $2\pi(x' + x)(x' - x)/\lambda r'$, dependent on the target location and equal to zero in the peak of the impulse response, i.e., for $x' = x$. Only at this point (and symmetrically for $x' = -x$) the phase of eq. (14) is identical to the strip mode value of $-4\pi r'/\lambda$.

In order to validate the above analysis, we have considered a simulation based on the system parameters of the SRTM mission that will operate with two Scan SAR sub-systems illuminating two sub-swaths each [5]. We considered three targets located in the farthest sub-swath, each at the same range and displaced in the azimuth direction so that each contributes to the overall burst. The resulting amplitude azimuth cross sections with and without antenna pattern compensation, are shown in figs 4 and 5 respectively. Note that side-lobe reduction has been achieved by multiplying, in time domain, the burst signal by a Hamming-0.54 weighting function [14]. Note also that for this system geometry the range migration effect is negligible.

We turn our attention to the phase of the point target impulse responses. To simplify the interpretation of the results we have **separately** plotted, in figs. 6a, 6b and 6c the azimuth dependent component of the phase, around the peak, for the targets A, B and C, labeled in fig. 4; the three curves are overlaid in fig. 7 to allow the comparison. The parabolic behaviour of the functions expected from eq. (14) is particularly evident in fig. 6b. Moreover all the phase functions cross the zero around the peak of the impulse response. Note also that, according to eq. (14), the parabolic phase term depends on the three variables x' , r' and x , therefore not only the range location of the target (as for the strip mode case) but also the azimuth location has an impact on the phase characteristics of the image impulse response (see fig. 7). It is also evident from fig. 7 that the azimuth phase variation from pixel to pixel can be quite large thus interpolation operations must be carefully carried out on the complex ScanSAR images. Moreover, in the interferometric case, even small misregistration effects between the image pair can lead to large errors in the phase of the interferogram.

Note also that, for the curves of fig. 7, the differences between the derived theory and the simulation results are always less than 0.009 rad.

In the next section a short analysis on the spectral properties of the ScanSAR data is presented in order to clarify the bandwidth characteristics of this signal.

III. Frequency-domain analysis

The starting point of this analysis is the evaluation of the Fourier transform of eq. (8):

$$\begin{aligned}
 A(\xi, r', x) &= FT[a(x' - x, r', x)] \\
 &= \int dx' a(x' - x, r', x) \exp[-j2\pi \xi x'] \\
 &= \int dq \exp[-j2\pi \xi x] \exp[-j2\pi \xi q] \exp\left[-j2\pi \frac{q^2}{\lambda r'}\right] w^2 \left[\frac{q}{X_S}\right] \cdot \\
 &\quad \cdot \text{rect}\left[\frac{q-x}{X_B}\right] \\
 &= \int dq \exp[-j2\pi \xi x] \exp[-j2\pi \Psi(q)] w^2 \left[\frac{q}{X_S}\right] \text{rect}\left[\frac{q-x}{X_B}\right] \quad (17)
 \end{aligned}$$

where $FT[\cdot]$ represents the Fourier transform operator, ξ is the azimuth spatial frequency often interpreted in terms of Doppler frequency, $q = x' - x$, anti

$$\Psi(q) = \xi q + \frac{q^2}{\lambda r'}. \quad (18)$$

In order to evaluate the integral in eq. (17), we apply the asymptotic expansion based on the stationary phase method (SPM), which is

particularly appropriate for signals with large time-bandwidth products [15] such as those from strip mode SAR systems. SPM may not be particularly appropriate for ScanSAR systems using particularly short bursts; however, since we are only interested in the spectral behaviour of the ScanSAR signal, we will assume the validity of the SPM and direct the interested reader to [15] for an extended analysis on the limit of validity of the SPM expansions.

The stationary phase approximation of eq. (17) yields (as usual, inessential factors are neglected):

$$A(\xi, r', x) \approx \exp[-j2\pi\xi x] \exp[-j2\pi\Psi(q_s)] w^2 \left[\frac{q_s}{X_S} \right] \text{rect} \left[\frac{q_s - x}{X_B} \right] \quad (19)$$

where the stationary phase point q_s is computed as follows:

$$\left. \frac{d\Psi(q)}{dq} \right|_{q_s} = \xi + \frac{2q_s}{\lambda r'} = 0 \quad \rightarrow \quad q_s = -\frac{\xi \lambda r'}{2}. \quad (20)$$

Using eq. (20) in (19) results in the following expression:

$$\begin{aligned} A(\xi, r', x) &\approx \exp[-j2\pi\xi x] \exp \left[j2\pi \frac{\xi^2 \lambda r'}{4} \right] w^2 \left[-\xi \frac{\lambda r'}{2X_S} \right] \text{rect} \left[\frac{\xi + \frac{2x}{\lambda r'}}{\frac{2X_B}{\lambda r'}} \right] \\ &= \exp \left[j2\pi \left(\frac{\xi^2 \lambda r'}{4} - \xi x \right) \right] w^2 \left[-\frac{\xi L}{2} \right] \text{rect} \left[\frac{\xi + \frac{2x}{\lambda r'}}{\frac{2X_B}{L X_S}} \right]. \end{aligned} \quad (21)$$

We note that the azimuth (spatial) spectrum is centered around the frequency $-2x / \lambda r'$ and its width $2X_B / LX_S$ explicitly depends on the burst duration.

The evacuation of the FT of eq. (9) via the SPM leads to:

$$G(\xi, \eta, r') \approx \exp\left[-j2\pi\frac{\xi^2\lambda r'}{4}\right] \text{rect}\left[\frac{\xi}{2}\right]. \quad (22)$$

By comparing the spectral widths of the functions in eqs. (21) and (22) it is evident that the burst nature of the Scan SAR signal causes a bandwidth reduction depending on the ratio X_B/X_S that is responsible for the ScanSAR azimuth resolution degradation already shown in eq. (16). This frequency domain formulation also illustrates the effect of a scan misregistration, say $\Delta x'$. In this case the burst window becomes $\text{rect}\left[(x' + \Delta x')/X_B\right]$ thus causing a spectral shift of the signal in eq. (21):

$$A(\xi, r', x) \approx \exp\left[j2\pi\left(\frac{\xi^2\lambda r'}{4} - \xi x\right)\right] w^2\left[-\frac{\xi L}{2}\right] \text{rect}\left[\frac{\xi + \frac{2x}{\lambda r'} - \frac{2\Delta x'}{\lambda r'}}{\frac{2X_B}{L X_S}}\right]. \quad (23)$$

This result, already demonstrated in [16], shows that in order to preserve the phase accuracy in multi-pass ScanSAR interferometry, we must account for the overlapping components of the azimuth data spectra in the presence of a scan misregistration.

The effect of a squint angle can be also easily shown. For data squinted at an angle ϕ_0 the antenna pattern has the form $w^2[(x' - x + r' \tan\phi_0)/X_S]$. In this case, eq. (21) becomes:

$$A(\xi, r', x) \approx \exp\left[j2\pi\left(\frac{\xi^2\lambda r'}{4} - \xi x\right)\right] \left| W\left[-\frac{L}{2}\left(\xi - \frac{2}{\lambda}\tan\phi_0\right)\right] \right| \cdot \text{rect}\left[\frac{\xi + \frac{2x}{\lambda r'}}{\frac{2X_B}{L X_S}}\right] \quad (24)$$

where the shift of the spectral envelope, caused by the squint angle, is evident.

1 V. Chirp z-transform based processing approach

Processing ScanSAR data using a standard range-Doppler approach is relatively inefficient due to the large zero padding required for azimuth compression. To understand why this is so, we observe that even though the burst length X_B is shorter than the synthetic antenna length X_S , the scatterers that contribute to a single burst are located in the larger region delimited, in the azimuth direction, by $-(X_B + X_S)/2 \leq x \leq (X_B + X_S)/2$ (see fig. 3). The above observation implies that the convolution operation in eq. (10), carried out on burst data of length X_B generates an image whose azimuth extent is $X_S + X_B$ ⁽³⁾. Since convolutions are efficiently carried out in the frequency domain via FFTs, this implies that the burst data must be first zero padded up to the dimension $X_S + X_B$.

An alternative, very efficient, method to process ScanSAR data is the SPECAN algorithm [6]. In this case the azimuth focusing is carried out by simply applying a phase multiplication operation and a Fourier transform step *involving the original burst data without any zero padding* (or a very limited padding to the nearest power of two for typical discrete FT codes). Strictly speaking, no range migration compensation is included in the basic SPECAN approach however, as previously mentioned, this is not a severe problem for most Scan SAR applications.

To better understand SPECAN ScanSAR processing it is important to emphasize the following: the ScanSAR transfer function bandwidth is $2X_B/X_S L$, seen in eq. (21), which is only a fraction of the strip mode bandwidth of $2/L$, seen in eq. (22). Since the data are sampled according to the spectral width of eq. (22), a Fourier (Doppler) domain

(3) However, as mentioned before, **only** targets located in the sub-interval $(X_B - X_S)/2 \leq x \leq (-X_B + X_S)/2$ **contribute** to the overall burst.

processing approach based on eq. (10) leads to an oversampled signal. This oversampling effect is avoided by using the SPECAN algorithm leading to increased computational efficiency.

Specifically applying the SPECAN algorithm to the burst signal in eq. (8) involves the following procedure: we multiply the burst signal by the factor $\exp\left[+j2\pi(x')^2 / \lambda r'\right]$ (referred to as the *deramping* step) followed by a Fourier transform, leading to (but for an unessential amplitude factor):

$$\begin{aligned}
\tilde{a}(\bar{\xi} - x, r', \bar{x}) &= FT \left\{ a(x' - x, r', x) \exp \left[j2\pi \frac{(x')^2}{\lambda r'} \right] \right\} \\
&= \exp \left[-j2\pi \frac{x^2}{\lambda r'} \right] \int dx' \text{rect} \left| \frac{x'}{X_B} \right| \exp \left[+j2\pi \frac{2x'x}{\lambda r'} \right] \\
&\quad \cdot \exp \left[-j2\pi \xi x' \right] \\
&= \exp \left[-j2\pi \frac{x^2}{\lambda r'} \right] \int dx' \text{rect} \left| \frac{x'}{X_B} \right| \exp \left[-j2\pi x' \left(\xi - \frac{2x}{\lambda r'} \right) \right] \\
&= \exp \left[-j2\pi \frac{x^2}{\lambda r'} \right] \text{sinc} \left[2\pi \frac{X_B}{2} \left(\xi - \frac{2x}{\lambda r'} \right) \right] \\
&= \exp \left[-j2\pi \frac{x^2}{\lambda r'} \right] \text{sinc} \left[\frac{2\pi X_B}{L X_S} (\bar{\xi} - x) \right]
\end{aligned} \tag{25}$$

where

$$\bar{\xi} = \xi X_S \frac{L}{2}. \tag{26}$$

Note that eq. (25) is different from eq. (13) in the term $\exp\left[+j2\pi(x')^2 / \lambda r'\right]$ [not present in eq. (25)] and for the variable $\bar{\xi}$ instead of x' (we also neglected the antenna pattern term $W^2[\cdot]$ whose effect can be compensated in the post-processing).

Because SPECAN algorithm is particularly relevant for its digital implementation, we consider the sampled version of eq. (25):

$$\tilde{a}(i\Delta\bar{\xi} - x, r', x) = \exp\left[-j2\pi\frac{x^2}{\lambda r'}\right] \text{sinc}\left[\frac{2\pi}{L}\frac{X_B}{X_S}(i\Delta\bar{\xi} - x)\right] \quad (27)$$

where i is the integer data index, $\Delta\bar{\xi}$ is the azimuth sampling frequency spacing, that, by assuming a spatial sampling $\Delta x'$ equal to the Nyquist limit $1/\Delta x' = 2/L$ [see eq. (22)], has the following expression:

$$\Delta\bar{\xi} = \Delta\xi X_S \frac{L}{2} = \frac{2/L}{X_B/\Delta x'} X_S \frac{L}{2} = \Delta x' \frac{X_S}{X_B} \quad (28)$$

with $\Delta\xi = (2/L)/(X_B/\Delta x')$ and where $X_B/\Delta x'$ is the integer number of samples for each burst. By finally replacing eq. (28) in (27) we obtain:

$$\text{ii}\left(i\Delta x' \frac{X_S}{X_B} - x, r', x\right) = \exp\left[-j2\pi\frac{x^2}{\lambda r'}\right] \text{sinc}\left[\frac{2\pi}{L}\frac{X_B}{X_S}\left(i\Delta x' \frac{X_S}{X_B} - x\right)\right] \quad (29)$$

which, except for the previously mentioned factor $w^2[i\Delta x'/X_S] \exp_{+j2\pi(i\Delta x'X_S/X_B)^2/\lambda r'}$, is the sampled version of eq. (13) without oversampling.

Although particularly attractive for its computational efficiency, because the processing involves a single FT restricted to the data length \mathbf{x}_B , it suffers from the presence of the range dependent factor $X_S \approx \lambda r'/L$ in the expression of $\Delta\bar{\xi}$ [see eq. (28)]. This term causes an undesirable range dependent scaling of the azimuth pixel dimension. This effect is generally compensated following the FT operation with an interpolation block that resamples to a constant azimuth pixel spacing. However, this interpolation step is not a trivial operation both in terms of computational efficiency and accuracy. Short interpolation kernels can introduce interpolation artifacts in the image while long interpolation kernels increase the computational requirements. The block diagram for the SPECAN procedure is shown in fig. 8. Different solutions that avoid this interpolation operation have been presented, recently, based on different combinations of a deramp Step with a

standard strip mode SAR processing algorithm [14,16]; in this case an accurate range cell migration compensation is also achieved.

We propose in the following an alternative solution based on a specific modification of the SPECAN algorithm; in our case the azimuth interpolation step is avoided by replacing the standard Fourier transform used in the SPECAN procedure, with a different one whose kernel, $\exp[-j2\pi\xi K(r') x']$, includes the range dependent scaling factor:

$$K(r') = \frac{r'_0}{r'}, \quad (30)$$

where r'_0 is a fixed range that is computed from the desired azimuth pixel spacing. In this case eq. (25) becomes:

$$\begin{aligned} \tilde{a}(\bar{\xi} - x, r', x) &= \int dx' a(x' - x, r', x) \exp\left[j2\pi \frac{(x')^2}{\lambda r'}\right] \exp[-j2\pi\xi K(r') x'] \\ &= \exp\left[-j2\pi \frac{x^2}{\lambda r'}\right] \int dx' \text{rect}\left[\frac{x'}{X_B}\right] \exp\left[+j2\pi \frac{2x'x}{\lambda r'}\right] \\ &\quad \cdot \exp[-j2\pi\xi K(r') x'] \\ &= \exp\left[-j2\pi \frac{x^2}{\lambda r'}\right] \text{sinc}\left[\frac{2\pi X_B}{L X_S} (\bar{\xi} - x)\right], \end{aligned} \quad (31)$$

where

$$\bar{\xi} = \xi X_S K(r') \frac{L}{2} = \xi X \frac{L}{2}, \quad (32)$$

with $X = \lambda r'_0 / L$. Note that in this case the sampling spacing $\Delta\bar{\xi}$ is range independent:

$$\Delta\bar{\xi} = \Delta x' \frac{X}{X_B} \quad (33)$$

Eq. (31) can be efficiently computed by applying the chirp z-transform algorithm that reduces the integration in eq.(31) to a convolution step. The core of the chirp z-transform algorithm is the following identity:

$$\begin{aligned} \exp[-j2\pi\xi K(r')x'] &= \exp[-j\pi K(r')\xi^2] \exp[-j\pi K(r')x'^2] \\ &\cdot \exp[j\pi K(r')(x' - \xi)^2]. \end{aligned} \quad (34)$$

Making use of the above identity in eq. (31) produces:

$$\begin{aligned} \tilde{a}(\bar{\xi} - x, r', x) &= \exp[-j\pi K(r')\xi^2] \int dx' \left| a(x' - x, r', x) \exp\left[j2\pi \frac{(x')^2}{\lambda r'} \right] \right. \\ &\quad \left. \cdot \exp[-j\pi K(r')x'^2] \right\} \exp[j\pi K(r')(x' - \xi)^2] \\ &= \exp\left[-j2\pi \frac{x^2}{\lambda r'}\right] \text{sinc}\left[\frac{2\pi X_B}{L X_S}(\bar{\xi} - x)\right]. \end{aligned} \quad (35)$$

From eq. (35) the processing strategy is clear: the burst signal is multiplied by the phase factor $\exp\left[-j\pi\left(K(r') - \frac{2}{\lambda r'}\right)x'^2\right]$ (which “fin’s a new deramp term), the result is convolved with the function $\exp[j\pi K(r')x'^2]$ and finally multiplied by $\exp[-j\pi K(r')\xi^2]$. The convolution operation included in eq. (35) can be carried using FFT codes and does not require zero padding of the burst data to the length $X_S + X_B$. However, a digital linear convolution is efficiently carried out using a circular convolution requiring a data doubling [7]: this leads, in our case, to an input data length equal to $2X_B$. Therefore the SPECAN with a chirp z-transform based algorithm is computationally competitive with respect to the standard convolution procedure, carried out in the azimuth frequency (Doppler) domain, until $X_S + X_B > 2X_B$.

We additionally note that the chirp z-transform based approach is fully phase-preserving but less efficient than the basic SPECAN since it requires a convolution step instead of a simple Fourier transform.

However, it does not require any additional interpolation in order to achieve a constant azimuth pixel spacing and maintains the basic simplicity of the SPECAN procedure. The block diagram of the chirp z-transform based algorithm is shown in fig. 9.

In order to increase the computational efficiency of the procedure shown in fig. 9 the FT of the term $\exp[j\pi K(r')x'^2]$ can be asymptotically evaluated at the expense of some accuracy. Note also that efficient FFT codes typically operate with power of two data lengths therefore, at the expense of some valid samples, the power of two zero padding can be used in some cases to avoid the burst data doubling. For example a 66 sample burst (possible selection in the SRTM case) zero padded up to 128 samples does not require any additional data doubling if the loss of one valid output sample is acceptable.

Finally we show some examples obtained applying the chirp z-transform based procedure of fig. 9. We used again the simulated data set generated for the experiments shown in section II. To show the capability of the proposed approach the azimuth cross sections of the focused targets generated with different pixel spacing are compared to the reference curves in fig. 4 (see fig. 10). Note again that these results have been obtained without any interpolation.

Conclusions

The characteristics of the impulse response of ScanSAR images have been investigated and the main differences, with respect to the strip mode case, have been elucidated. In particular it has been shown that in addition to well-known amplitude and resolution effects of burst discontinuities the phase of ScanSAR data is parabolically dependent on the azimuth target location. Therefore, the impact on preserving the phase in complex SAR imagery, when for example resampling or framing interferometric or polarimetric products, is great. For example, in the SRTM case, a misregistration of a 1/16th of pixel for a target in the center of the swath and at the edge of the image obtained from the burst, leads to a phase error in the interferogram of more than 40° , given a phase fidelity of only 8° ; clearly this error is not acceptable.

A new phase-preserving solution for ScanSAR data processing has been also presented. It maintains the simplicity and most of the efficiency of the SPECAN approach but generates images with constant azimuth pixel spacing without any interpolation; moreover, the image azimuth pixel dimension can be chosen to match the user requirements. This approach represents a valid processor candidate for phase-preserving ScanSAR data processing as in the SRTM case.

Acknowledgments

We want to thank G. Franceschetti for his support and R. M. Goldstein, M. Jin, C. Werner and S. Buckley for the interesting discussions had on this topic. We also thank G. Fornaro that provided the strip mode simulator code and S. J. Shaffer, E. Chapin and E. Gurrola for their help. This work has been done while Riccardo Lanari was visiting the Jet Propulsion Laboratory with a grant of the Italian CNR.

References

- [1] Elachi C., *Introduction to the Physics and Techniques of Remote Sensing*, John Wiley & Sons, New York, 1987.
- [2] Curlander J. C., McDonough R. N., *Synthetic Aperture Radar Systems and Signal Processing*, John Wiley & Sons, New York, 1991.
- [3] Tomiyasu K., Conceptual Performance of a Satellite Borne, Wide Swath Synthetic Aperture Radar, *IEEE Trans. on Geosci and Remote Sensing*, vol. 19, 108-116, 1981.
- [4] Moore K., Claassen J. P., Lin Y. H., Scanning Spaceborne Synthetic Aperture Radar with Integrated Radiometer, *IEEE Trans. on Aerospace and Electron. Syst.*, vol. 17, 410-420, 1981.
- [5] Kobrick M., Shuttle Radar Topography Mission: Data Products, Mission and System Requirements, JPL Technical Report N. D-13743, 1996.
- [6] Sack M., Ito M. R., Cumming I. G., Application of efficient linear FM matched filtering algorithms to synthetic aperture radar processing, *IEE Proc. part. F*, vol. 132, 45-57, 1985.
- [7] Rabiner L. R., Schafer R. W., Rader C. M., The chirp z-transform and its applications, *Bell System Tech. j.*, vol. 48, 1249-1292, 1969.
- [8] Raney R. K., Doppler properties of radars in circular orbits, *Int. J Remote Sensing*, vol. 7, 1153-1162, 1985.
- [9] Bamler R., Eineder M., ScanSAR processing Using Standard High Precision SAR algorithms, *IEEE Trans. on Geosci and Remote Sensing*, vol.34, 212-218, 1996.
- [10] Raney R. K., Runge H., Bamler R., I. G. Cumming, F. H. Wong, Precision SAR processing Using Chirp Scaling, *IEEE Trans. on Geosci and Remote Sensing*, vol.32, 786-799,1994.
- [11] Cafforio C., Prati C., Rocca F., SAR data focusing using seismic migration techniques, *IEEE Trans. on Aerospace and Electron. Syst.*, vol. 27, 194-207, 1991.
- [12] Franceschetti G., Lanari R., Marzouk E. S., A New Two-Dimensional Squint Mode SAR Processor, *IEEE Trans. on Aerospace and Electron. Syst.*, vol. 32, 854-863,1996.

- [13] Jin M. Y., Wu C., A SAR correlation algorithm which accomodates large range migration, IEEE Trans. on Geosci and Remote Sensing, vol.22, 592-597, 1984.
- [14] Mittermayer J., Moreira A., Davidson G., Bamler R., *SIR-C ScanSAR processing*, DLR report 96-25, 1996.
- [15] Copson F. T., *The Asymptotic Expansion of a Function Defined by a Definite Integral or Contour Integral*, The Admiralty, London, S. R. E./ACS 106, 1946.
- [16] Monti Guarnieri A., Prati C., ScanSAR focusing and Interferometry, IEEE Trans. on Geosci and Remote Sensing, vol.34, 1029-1038, 1996.

Captions of the figures

Fig. 1 Reference coordinate system.

Fig. 2 ScanSAR operating mode for a two sub-swaths case.

Fig. 3 ScanSAR geometry in the (x, r) plane.

Fig. 4 Azimuth amplitude cross section with antenna pattern correction; three targets are present, labeled A, B and C, respectively.

Fig. 5 Azimuth amplitude cross section without antenna pattern correction.

Fig. 6a Azimuth phase cross section around the peak of target A of fig. 4.

Fig. 6b Azimuth phase cross section around the peak of target B of fig. 4.

Fig. 6c Azimuth phase cross section around the peak of target C of fig. 4; a simple unwrapping procedure has been applied in this case.

Fig. 7 Overlaid plots of figs, 6a, 6b and 6c.

Fig. 8 SPECAN algorithm block diagram for ScanSAR azimuth focusing.

Fig. 9 Chirp z-transform based SPECAN algorithm block diagram.

Fig. 10 Azimuth amplitude cross sections with antenna pattern correction obtained by applying the algorithm of Fig. 9. Continuous line is coincident with the curve in fig. 4, '+' and '*' are obtained with a sample spatial dimension six and nine times larger than that of fig. 4 (here referred to as $\Delta x'$), respectively.

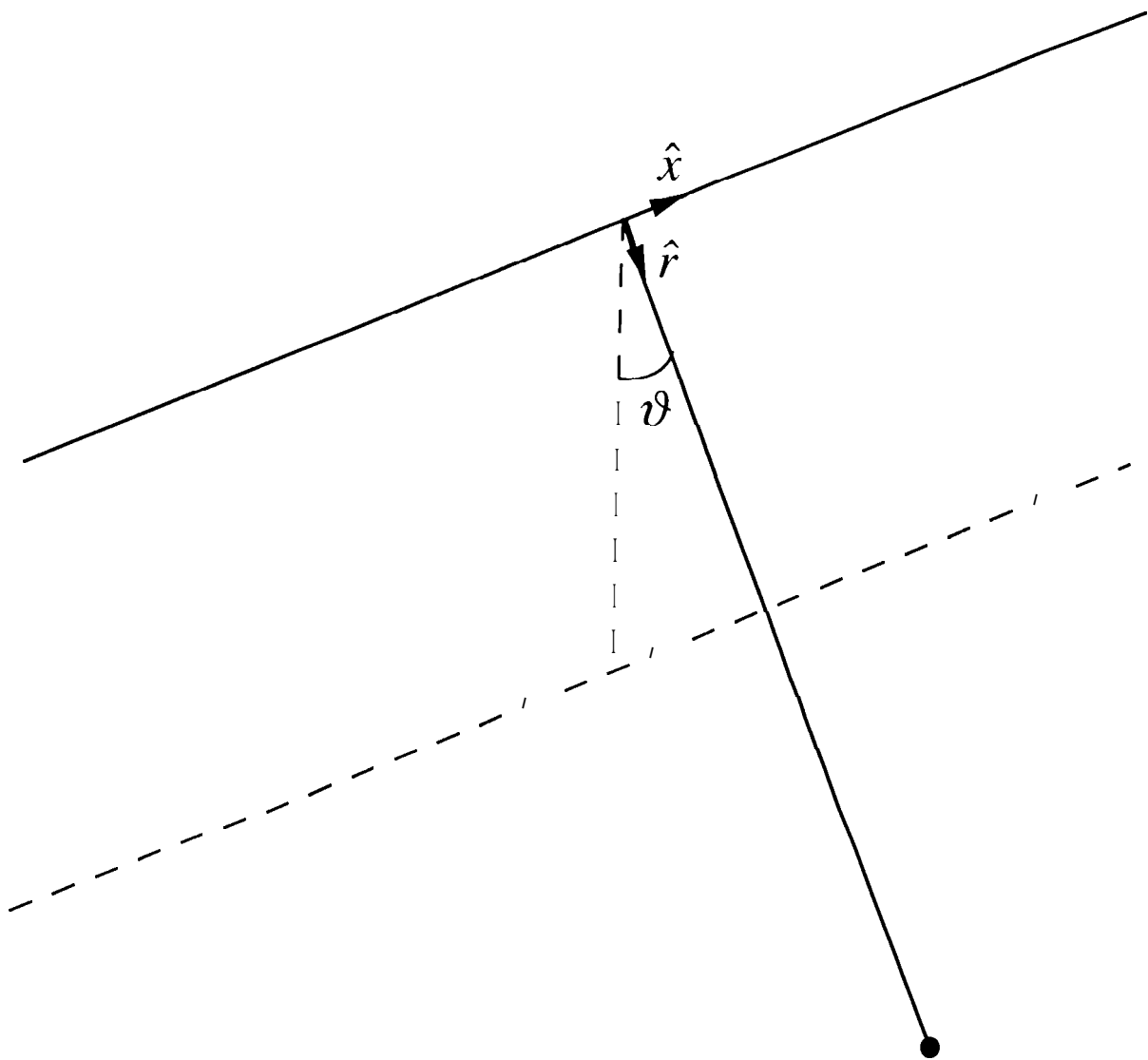


FIG. 1

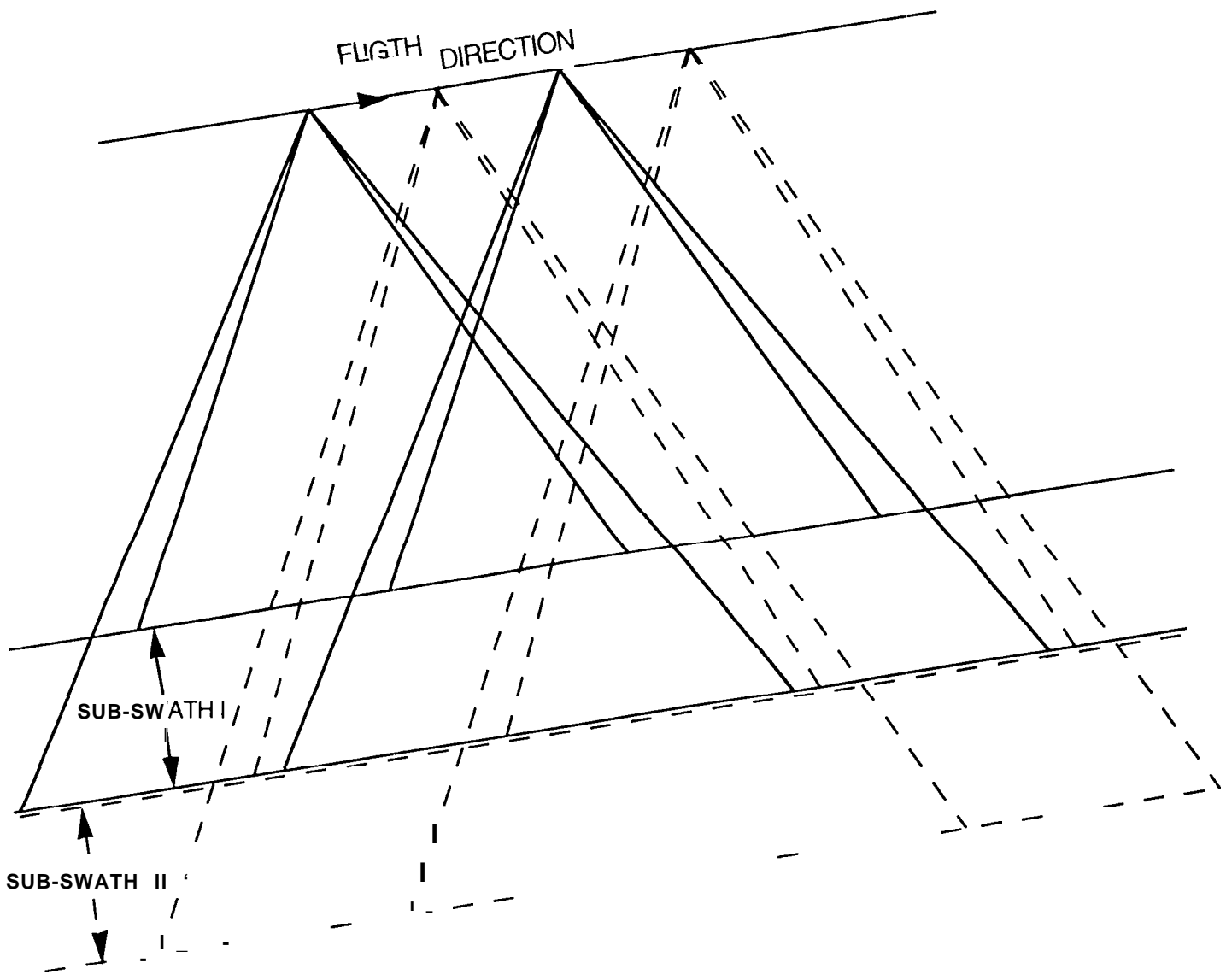


FIG. 2

— BURST START
- · BURST END

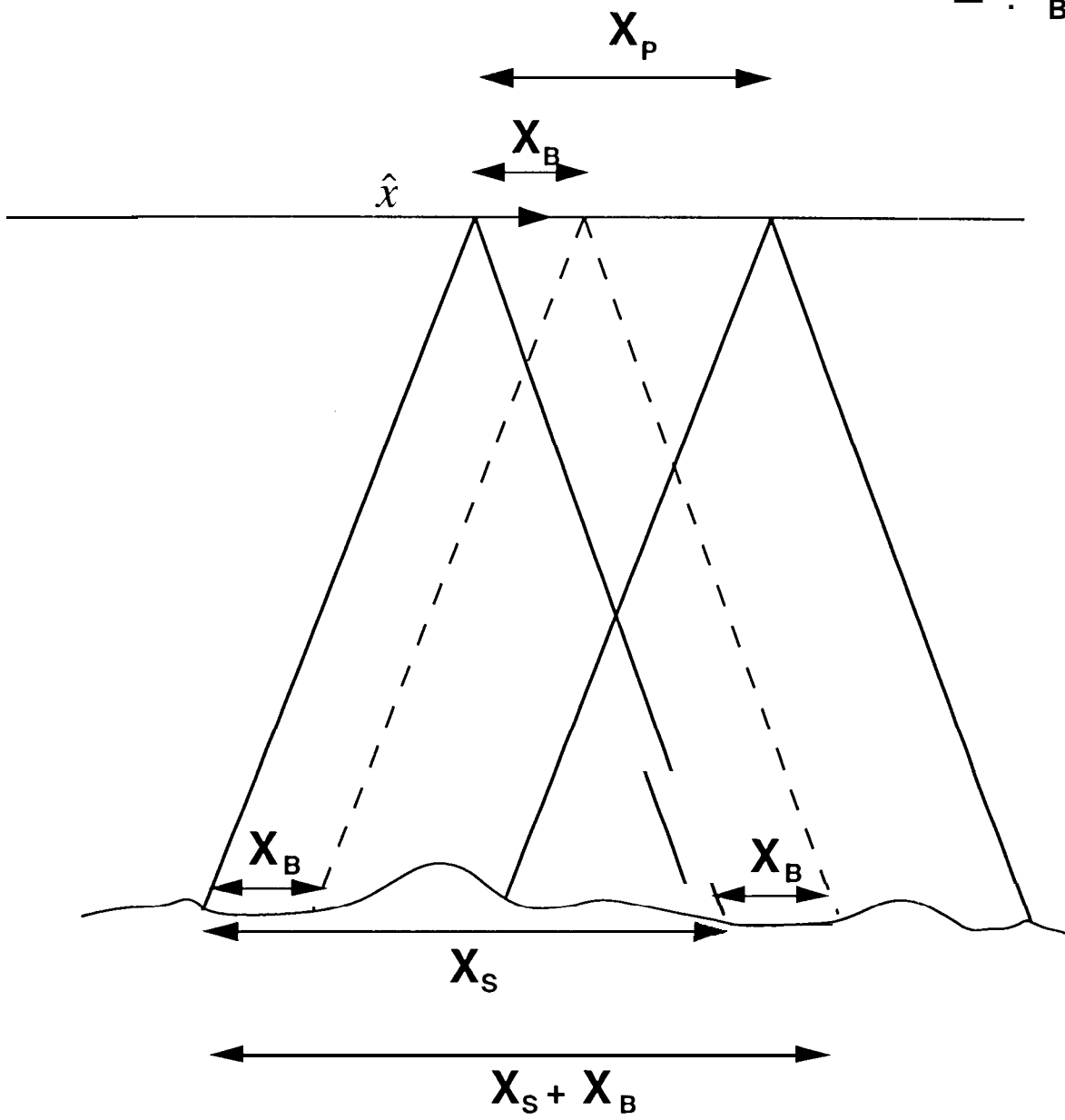


FIG. 3

[ARBITRARY
UNITS]

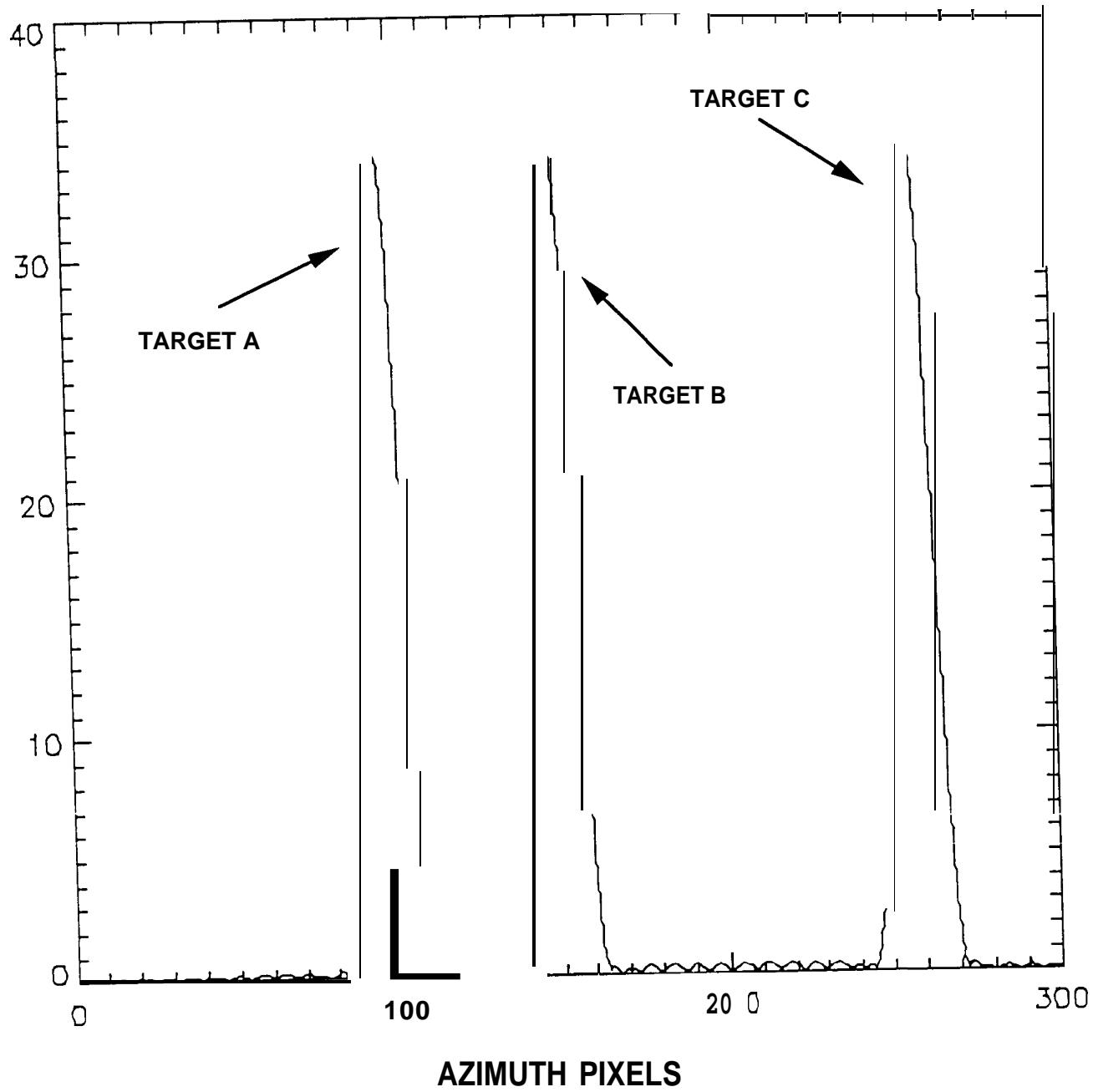


Fig. 4

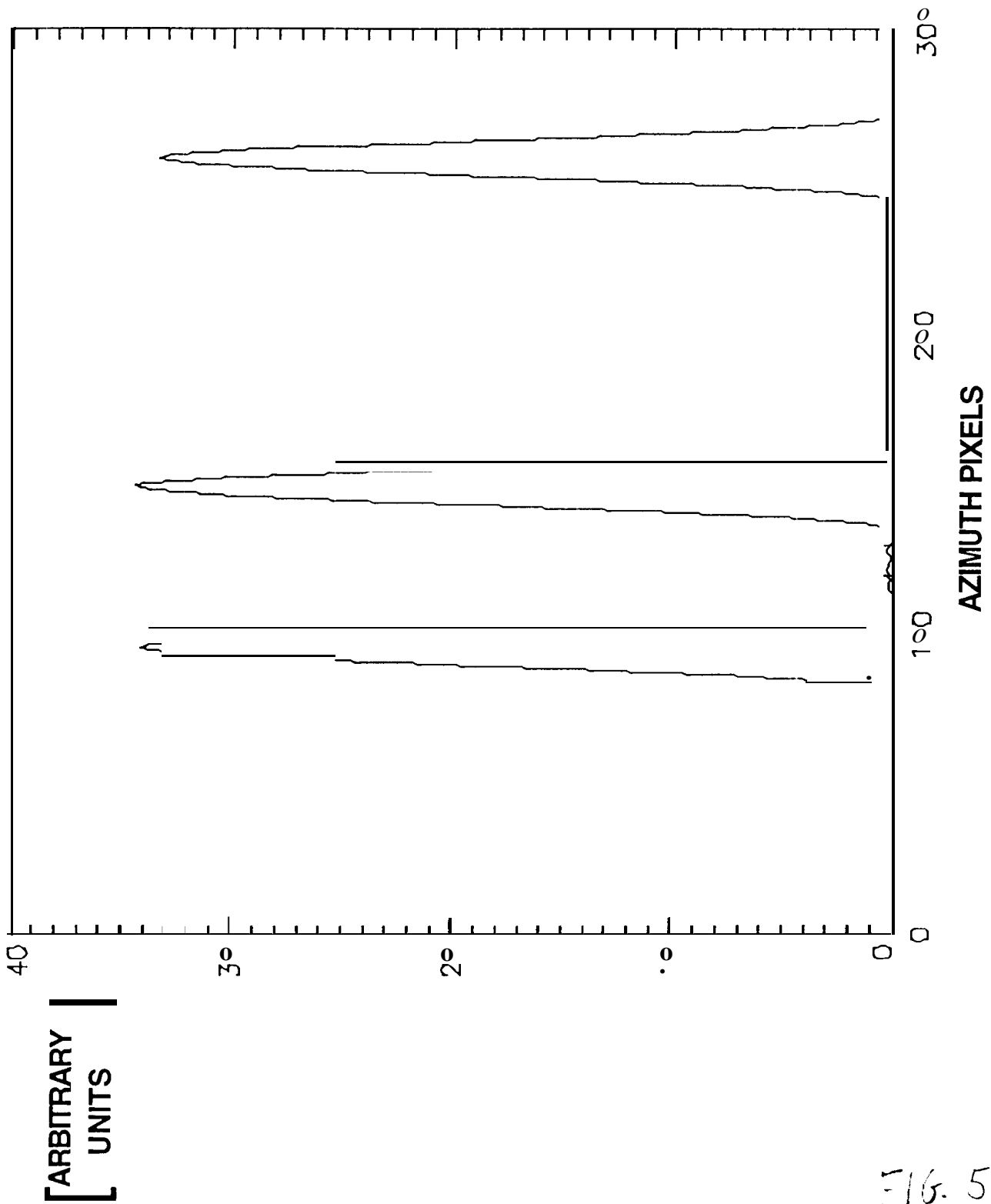


FIG. 5

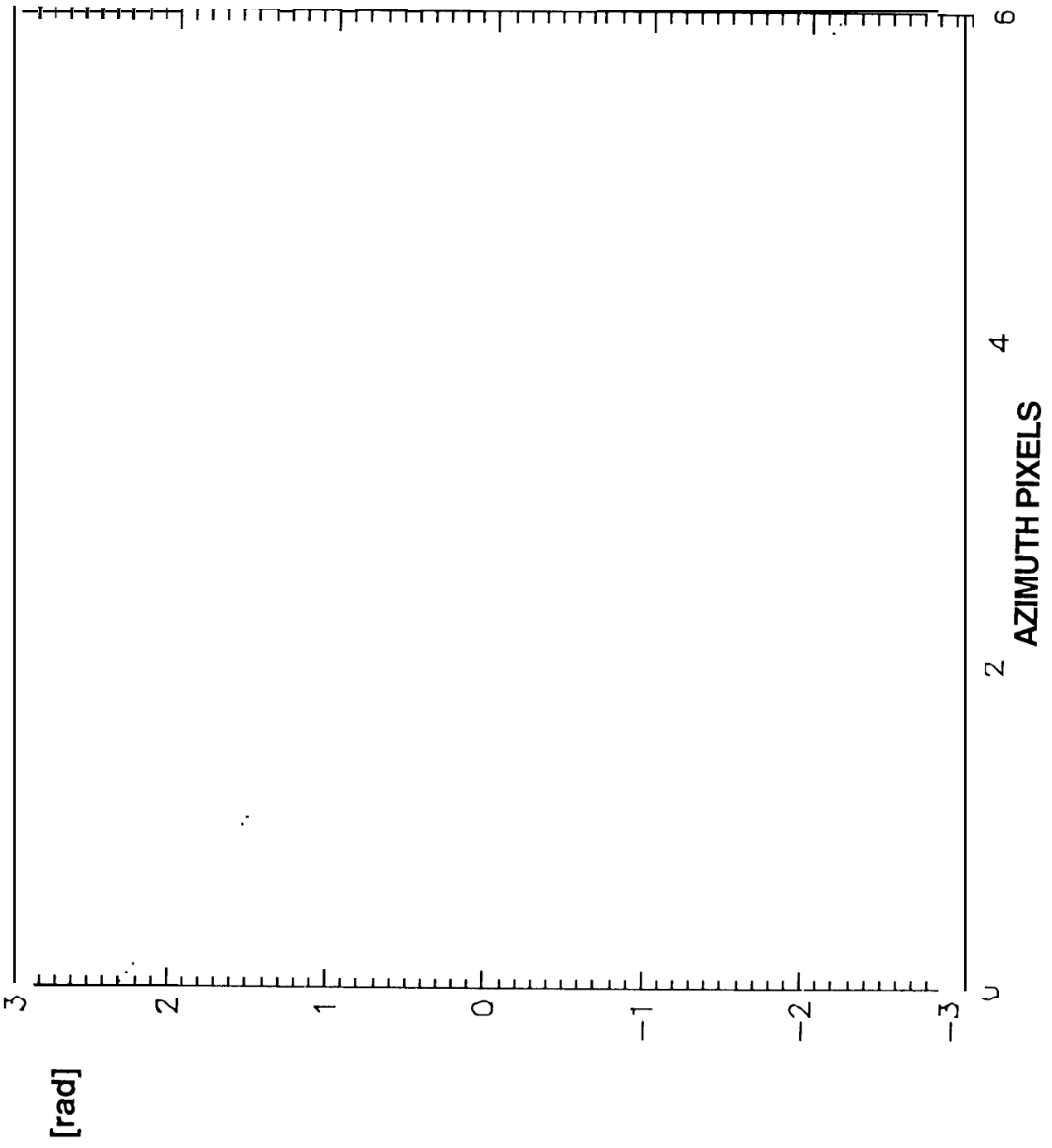
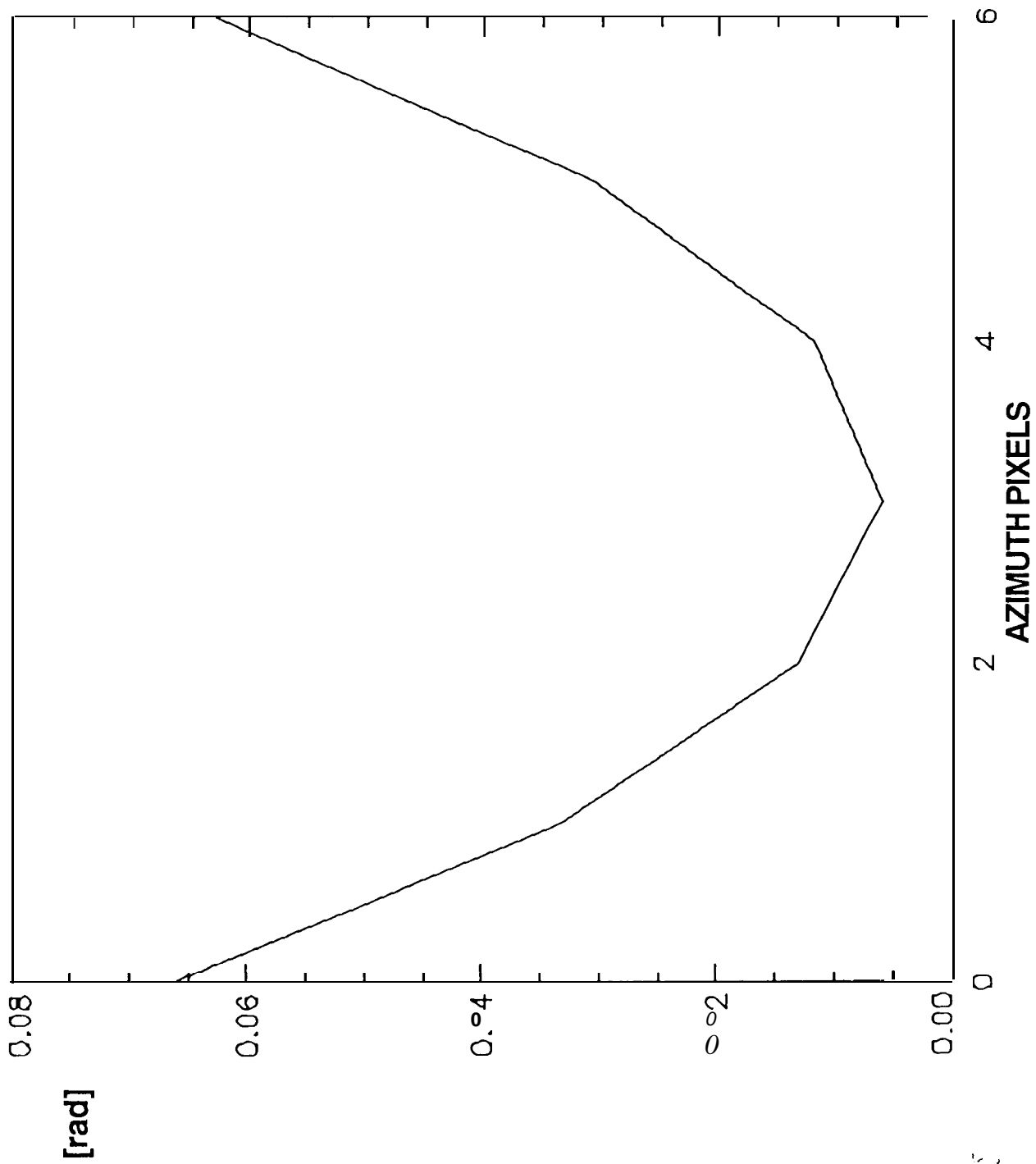


FIG. 2A



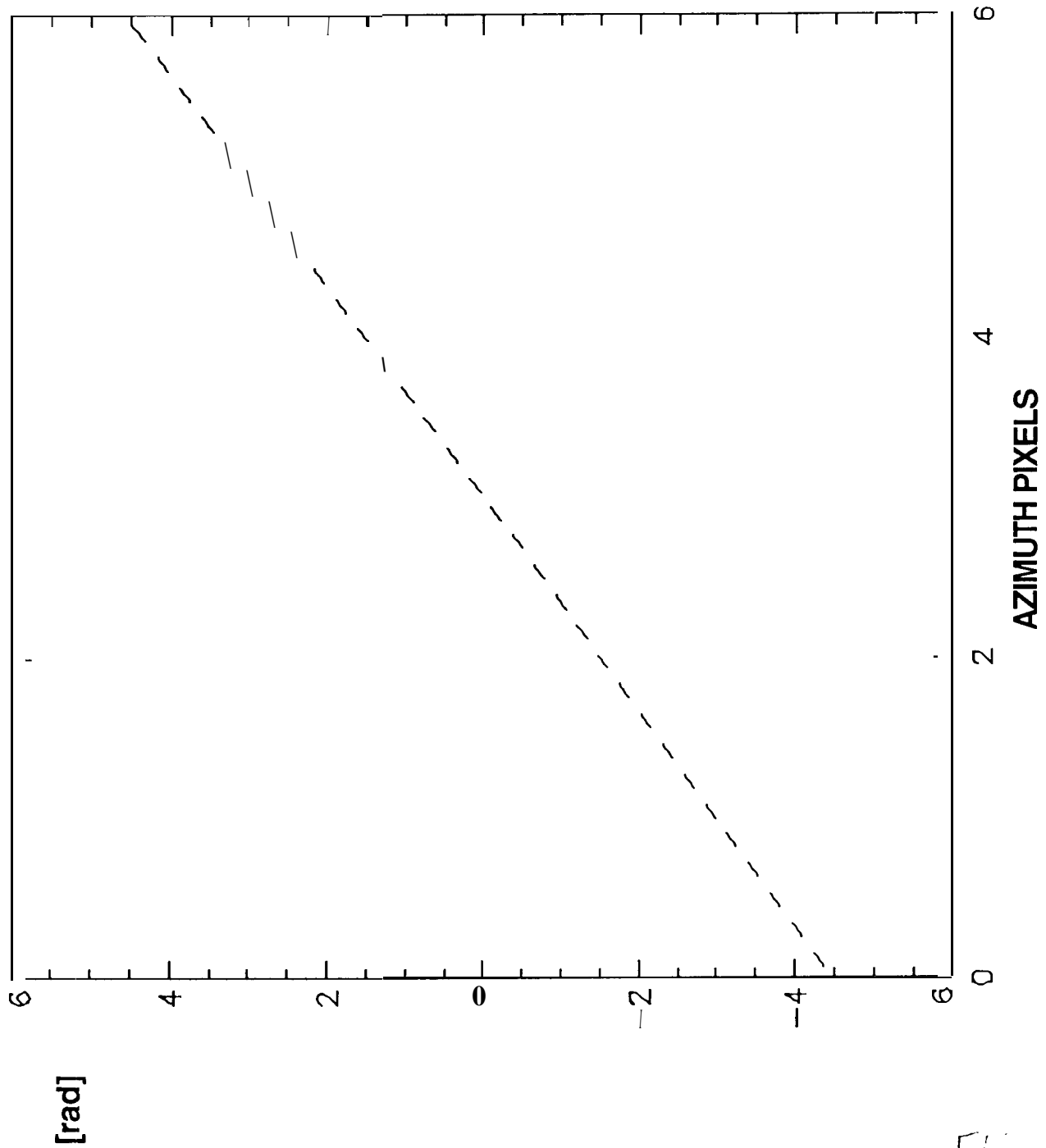


FIG. 5C

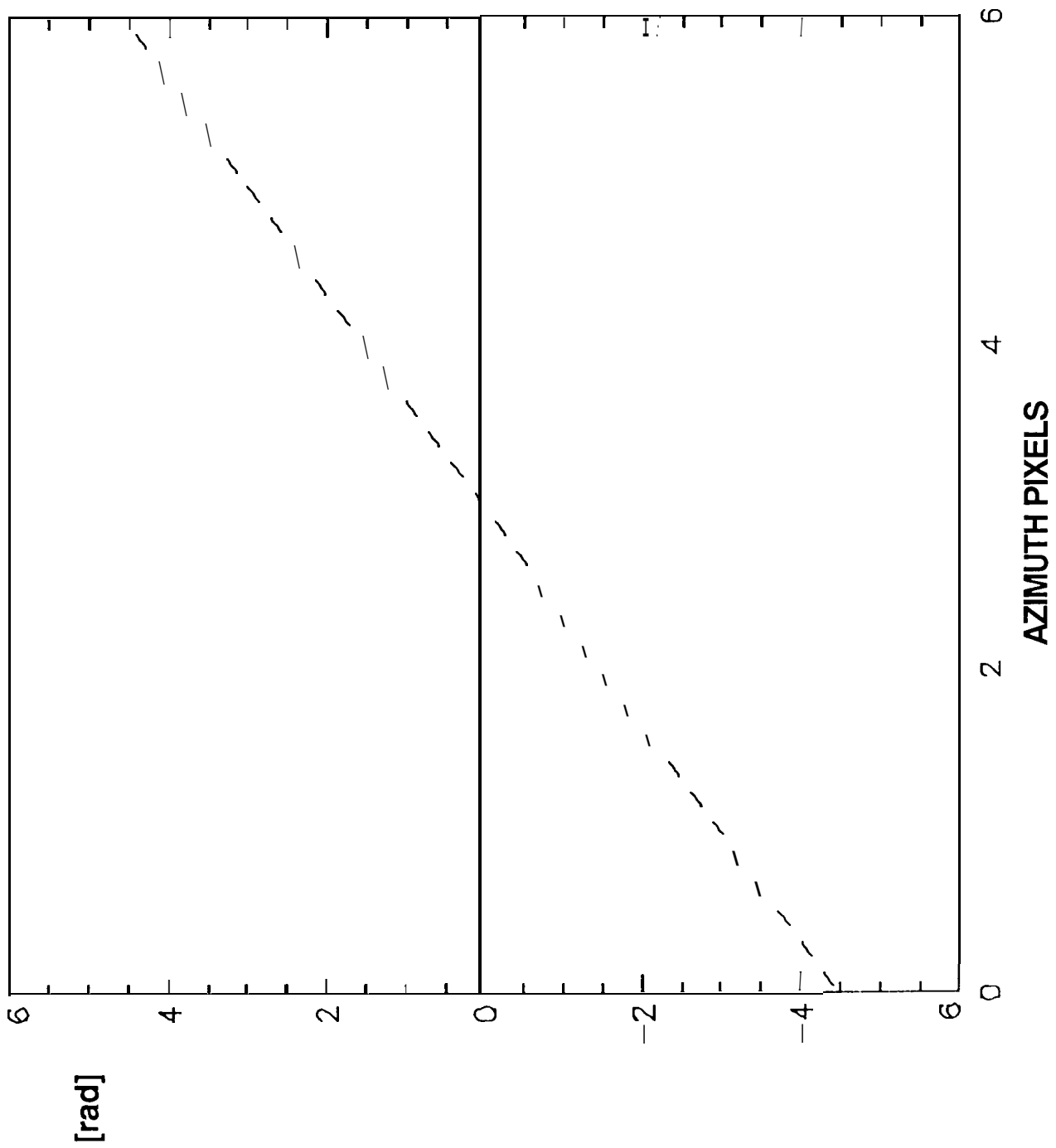


FIG. 7

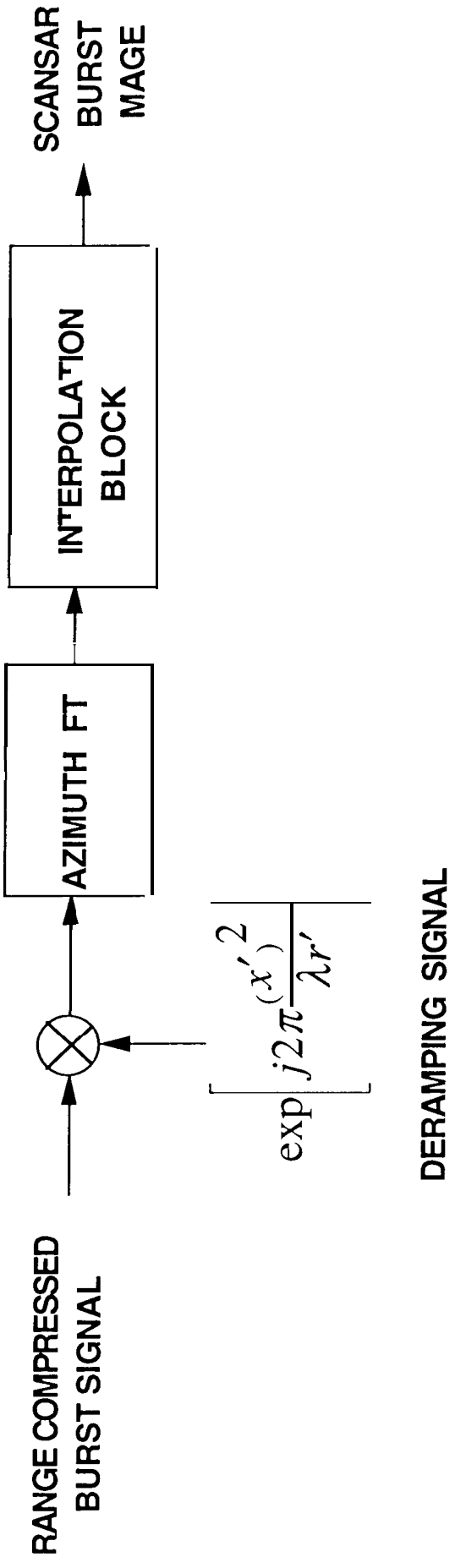


FIG. 2

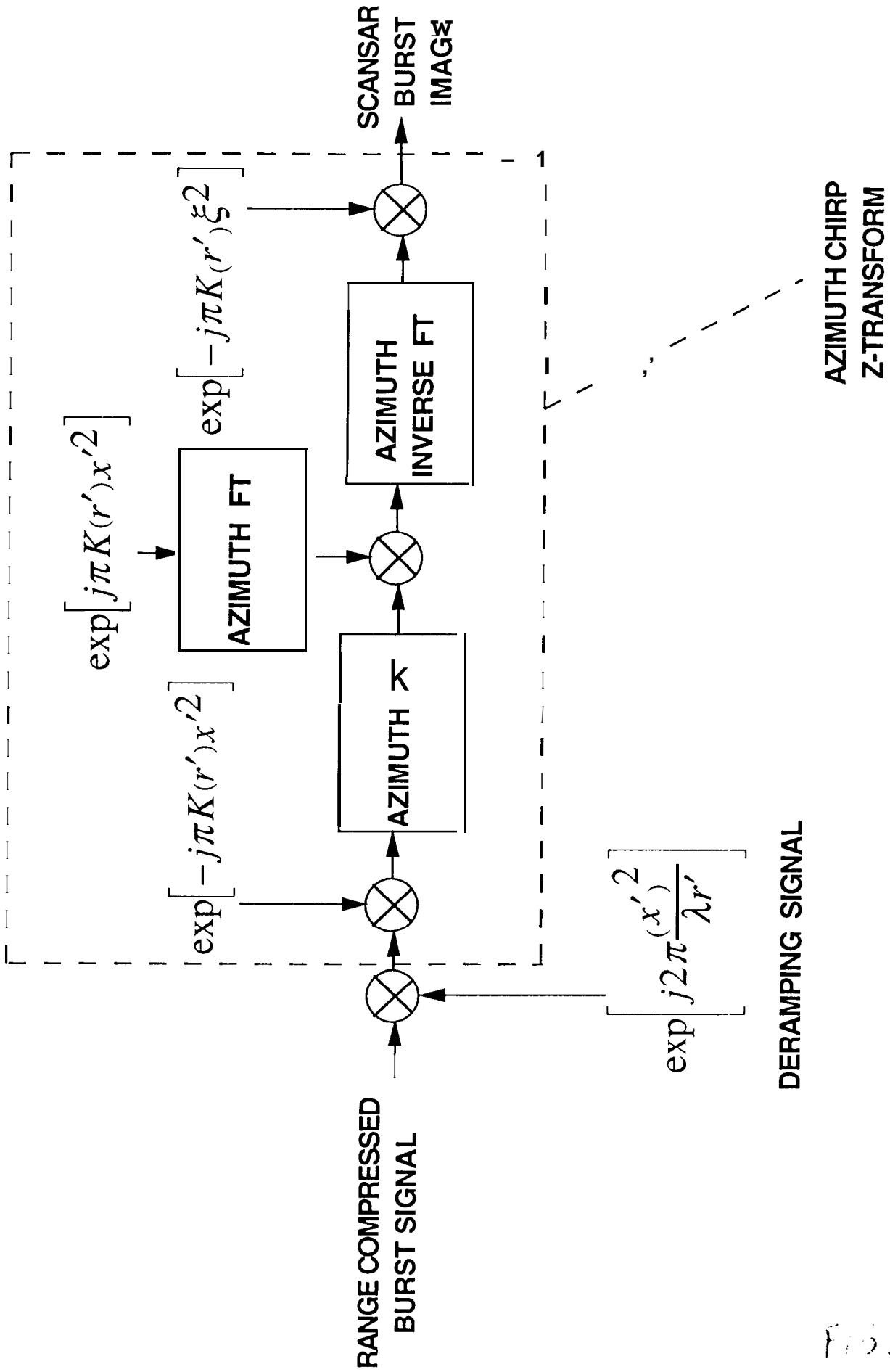


FIG. 1

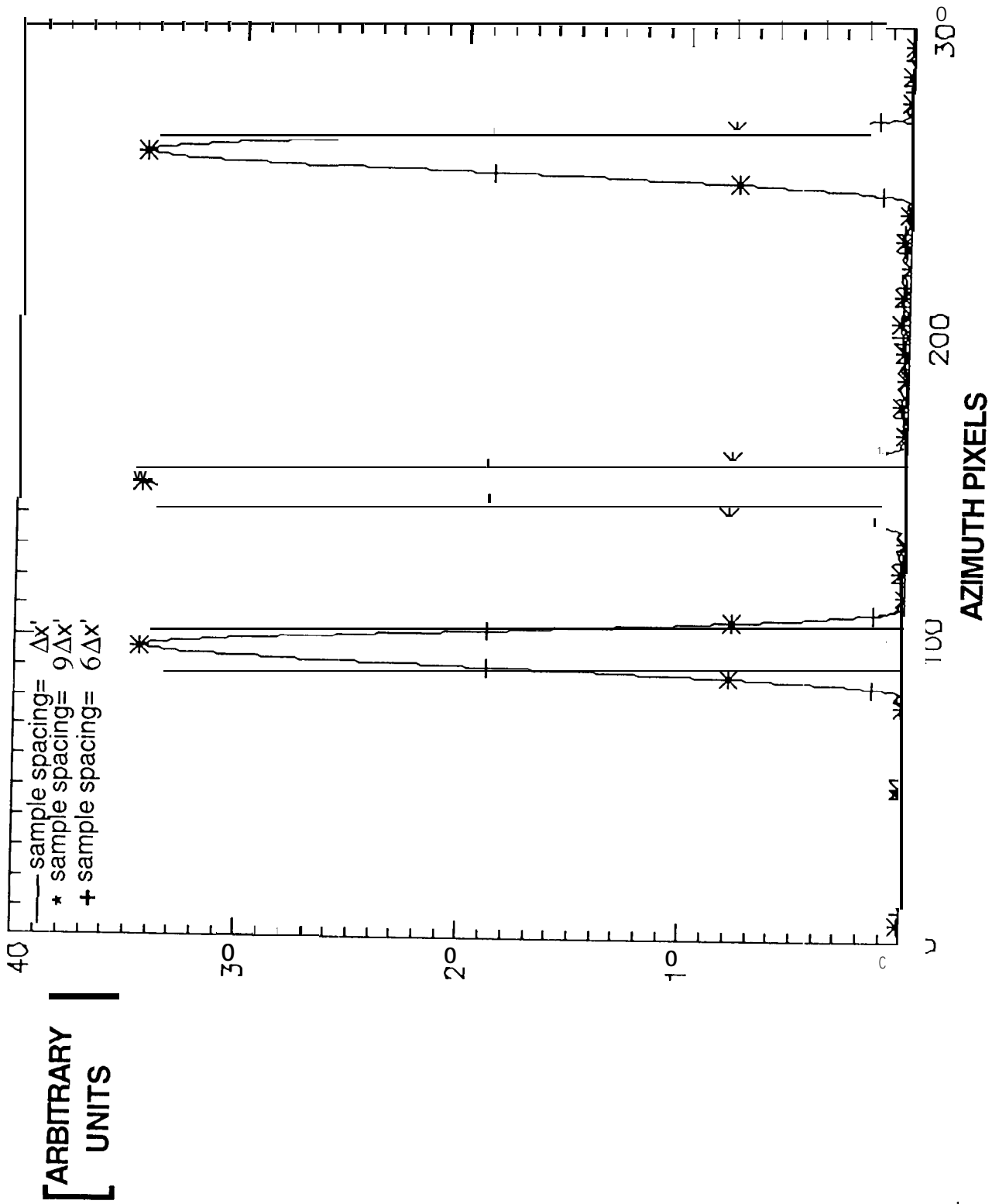


FIG. 10